

# Determination of Volumetric Mass Transfer Coefficient in Gas-Solid-Liquid Stirred Vessels Handling High Solids Concentrations: Experiment and Modeling

*Davoody, Meysam; Abdul Raman, Abdul Aziz\*<sup>+</sup>; Asgharzadeh Ahmadi, Seyed Ali;  
Binti Ibrahim, Shaliza*

*Department of Chemical Engineering, Faculty of Engineering, University of Malaya, 50603 Kuala Lumpur,  
MALAYSIA*

*Parthasarathy, Rajarathinam*

*School of Civil, Environmental, and Chemical Engineering, RMIT University, City Campus 3001, AUSTRALIA*

**ABSTRACT:** Rigorous analysis of the determinants of volumetric mass transfer coefficient ( $k_{LA}$ ) and its accurate forecasting are of vital importance for effectively designing and operating stirred reactors. Majority of the available literature is limited to systems with low solids concentration, while there has always been a need to investigate the gas-liquid hydrodynamics in tanks handling high solid loadings. Several models have been proposed for predicting  $k_{LA}$  values, but the application of neuro-fuzzy logic for modeling  $k_{LA}$  based on combined operational and geometrical conditions is still unexplored. In this paper, an ANFIS (adaptive neuro-fuzzy inference system) model was designed to map three operational parameters (agitation speed (RPS), solid concentration, superficial gas velocity (cm/s)) and one geometrical parameter (number of curved blades) as input data, to  $k_{LA}$  as output data. Excellent performance of ANFIS's model in predicting  $k_{LA}$  values was demonstrated by various performance indicators with a correlation coefficient of 0.9941.

**KEYWORDS:** Artificial intelligence-based modeling; Adaptive neuro-fuzzy inference system; Artificial neural networks; Volumetric mass transfer coefficient; Stirred vessels.

## INTRODUCTION

Three-phase (gas-liquid-solid) stirred reactors are commonly used in many chemical and biochemical process industries such as wastewater treatment, fermentation, hydrogenation, chlorination, mining processing and etc[1-8].

The volumetric gas-liquid mass transfer coefficient ( $k_{LA}$ ) is considered as one of the major parameters

in designing and operating gas-liquid-solid reactors [9, 10]. Many reviews on gas-liquid reactions and their mass transfer measurement methods have been carried out [11-13]. For example, many investigations on oxygen mass transfer into the water were summarized by Nienow [14]; Effects of impeller speed (300-600 rpm), gas flow rate

---

\* To whom correspondence should be addressed.

+ E-mail: azizraman@um.edu.my

1021-9986/2018/3/195-212

18\$/6.08

(8.92-33.81 cc/s) and liquid phase viscosity were investigated in a study by *Puthli et al.* [15]. Besides, the oxygen transfer rate in bioprocesses was studied by *Garcia-Ochoa & Gomez* [16] by reviewing the measurement methods and main empirical equations of  $k_{LA}$ . They considered impeller speed, type and number of impellers and gas flow rate as the main parameters in scale-up and design of stirred vessels for bioprocesses.

Presence of solids can influence  $k_{LA}$ . It has been reported that the settling of solid decreases the volumetric gas-liquid mass transfer coefficient in three-phase systems [17, 18]. In another study, *Mehta and Sharma* [19] reported a direct relationship between volumetric gas-liquid mass transfer coefficient and concentration of solids. In this regards, *Gentile et al.* (2003) [20] explained that the presence of solids increased specific gas-liquid interfacial area by causing break-up in large bubbles. *Kawase et al.* [21] measured the gas-liquid mass transfer in a Newtonian and non-Newtonian fluid. They found that the addition of solid particles increased the value of  $k_{LA}$  in water and decreased it in carboxymethyl cellulose aqueous solution.

*Tagawa et al.* [22] studied the effect of two types of floating solid particles on gas-liquid mass transfer in a stirred tank with a diameter of 0.2m. They reported that the increase in impeller speed increased the solid particles dispersion within the tank and the presence of floating solid decreased the power consumption due to decreased slurry density. However, the loading of a floating particle in the tank reduced the value of volumetric gas-liquid mass transfer coefficient in this study. They mentioned that it could be due to the decrease in the gas-liquid interfacial area. In addition, the floating solids increased the tendency of bubble coalescence and caused large bubble formation which reduced gas hold-up and volumetric gas-liquid mass transfer coefficient eventually.

For modeling, mathematical correlations were proposed to predict  $k_{LA}$  with respect to specific power input (P/V) [23-27]. Generally, it is difficult to propose a mathematical model capable of including all factors involved in a particular process. If the problem contains many independent variables, regression methods cannot be used due to loss of accuracy and increased number of variables in the regression (linear, non-linear, exponential, etc.) [28].

Due to the major drawbacks, Artificial Neural Networks (ANN) has been proposed to replace the conventional modeling. ANN does not rely on

assumptions concerning the nature of phenomenological mechanism but defines the mathematical equations and correlations. Efficiencies of ANN and mathematical models in predicting mass transfer coefficient have been compared in various studies and superior performance of ANN has been reported by all authors. Table 1 lists the major proposed ANN models for determining  $k_{LA}$ .

Despite its capabilities, ANN suffers from some drawbacks that limit its applications. The main issue with ANN is lack of interpretation. ANN failed to capture the causal relationships between the major system components and improve the explicit knowledge of the user [29]. Based on the report, ANN did not show satisfactory results in extrapolation.

Later, *Jang* [35] introduced Adaptive Neuro-Fuzzy Inference Systems (ANFIS) which is basically a combination of neural networks and fuzzy concepts. The new technique removes the major problems of both ANN (lack of interpretation) and fuzzy logic (adaptivity) systems and includes the main benefits. Various authors have reported satisfactory performance of ANFIS in different areas of chemical engineering such as membrane separation process, heat transfer, biodegradation, distillation, supercritical fluid extraction, and emulsion formation [36-45].

In accordance with the authors' knowledge, there is no reliable report in the available literature regarding the application of ANFIS in predicting  $k_{LA}$  based on a combination of operational and geometrical parameters. Therefore, a comparative work was carried out in this study to identify the most reliable model for predicting mass transfer coefficient in stirred vessels. In the first part of the study, experiments were carried out to determine  $k_{LA}$  in different conditions. Agitation speed (RPS), solid concentration, superficial gas velocity (cm/s), and a number of curved blades were selected as the main variables. The gathered experimental data was used in the second part of the study to build two artificial intelligence-based models, using ANN and ANFIS respectively. The last part of the study was devoted to compare the accuracy of the two models to identify the most reliable one.

## EXPERIMENTAL SECTION

### Experiment

Rushton turbine is widely employed for gaseous dispersion in multiphase systems [46-51]. However,

Table 1: The proposed ANN models for agitated vessels in literature.

Authors	Studied system	Input variables	Output variable(s)	Developed Models	Accuracy indicator(s)	Remarks
[29]	OD of Carica Papaya .L	Temperature (°C) Solution concentration (%) Agitation speed (RPM)	WR SG WL	ANN RSM ANN RSM	RMSE = 0.023 RMSE = 0.154 RMSE = 0.03 RMSE = 0.051 RMSE = 0.138 RMSE = 0.123	The results of ANN model indicated that it was much more robust and accurate in estimating the values of dependent variables when compared to the RSM model
[30]	OD of Kaffir lime peel	Solute concentration (%) Temperature (°C) Immersion time (h)	WL SG	ANN	MSE = 6.5813 R <sup>2</sup> = 0.9745 MSE = 5.934 R <sup>2</sup> = 0.9632	ANN was found suitable for predicting WL and SD during OD process of kaffir lime peel
[31]	Mass transfer in stirred vessels	Stirrer speed (s <sup>-1</sup> ) Superficial gas velocity (m/s) Consistency index (Pa.s <sup>n</sup> ) Flow index	k <sub>L</sub> a	ANN	R <sup>2</sup> = 0.98	The use of neural networks presented an alternative to classical models using regression techniques
[32]	CO <sub>2</sub> absorption into aqueous DETA	Gas phase concentration (%) Inert gas load (kmol/m <sup>3</sup> h) Liquid flow rate (m <sup>3</sup> /m <sup>2</sup> h) Solvent concentration (kmol/m <sup>3</sup> ) CO <sub>2</sub> loading (mol CO <sub>2</sub> / mol amine) Feed temperature (°C)	k <sub>L</sub> a	ANN	AAD% = 7.6	Results demonstrated that ANN model was suitable for predicting the absorption performance of packed columns
[33]	OD of apple	Temperature (°C) Concentration of osmotic solution (Brix) Immersion time (h) Surface (cm <sup>2</sup> )	WR SG	ANN	MSE = 13.9 R <sup>2</sup> = 0.96 MSE = 4.4 R <sup>2</sup> = 0.89	ANN performed better when compared to linear multi-variable regression

OD: Osmotic Dehydration

n: Flow index in a power-law model

WR: Weight Reduction

AAD: Absolute Average Deviation

SG: Solid Gain

R<sup>2</sup>: Correlation Coefficient WL: Water Loss

MSE: Mean Square Error

certain drawbacks such as reduction in power input with gassing due to the ventilated cavity formation limit its applications [52, 53]. A new design called hollow blade or Curved Blade (CB) was therefore introduced by [54]. The new design offers a higher mass transfer coefficient (almost 20%) and better power draw stability over Rushton turbine [55]. With reference to the mentioned points, CB was selected as the impeller in this study. Table 2 lists the specifications of the impeller and Fig. 1 reflects its design.

In this study, the mass transfer coefficient was studied as a function of superficial gas velocity, solid percentage, impeller rotational speed, and a number of curved blades. An experimental rig was designed and fabricated for this study. Fig. 2 illustrates this rig followed by Table 3 listing different parts of the apparatus.

The tank was made of scratch-proof Perspex material with 5 mm thickness. Four equally spaced baffles with a length of 4 cm (0.1D) were attached along the entire depth of the tank to minimize the vortex effects. Bottom

of the tank was flat and the top of the tank was kept open for all experiments.

Agitation was provided by a shaft placed at the vertical axis of the tank and driven by a 3.0 kW motor. The motor shaft was connected to the impeller via a shaft coupling. A 4.0 kW-frequency inverter was used to vary the agitation speed. Experiments were conducted from 300 to 1200 RPM (5-20 RPS). A ring sparger made of copper tubing that had a similar outer diameter as the impeller was chosen. Equally distanced holes of 2 mm diameter were made only at the bottom of the ring to avoid solid particles from blocking the sparger hole.

Geometrical dimensions of the stirred vessel used in this study were selected after identifying the most common fractions and ratios in the relevant literature. These dimensions are listed in Table 4.

#### Volumetric mass transfer coefficient measurement

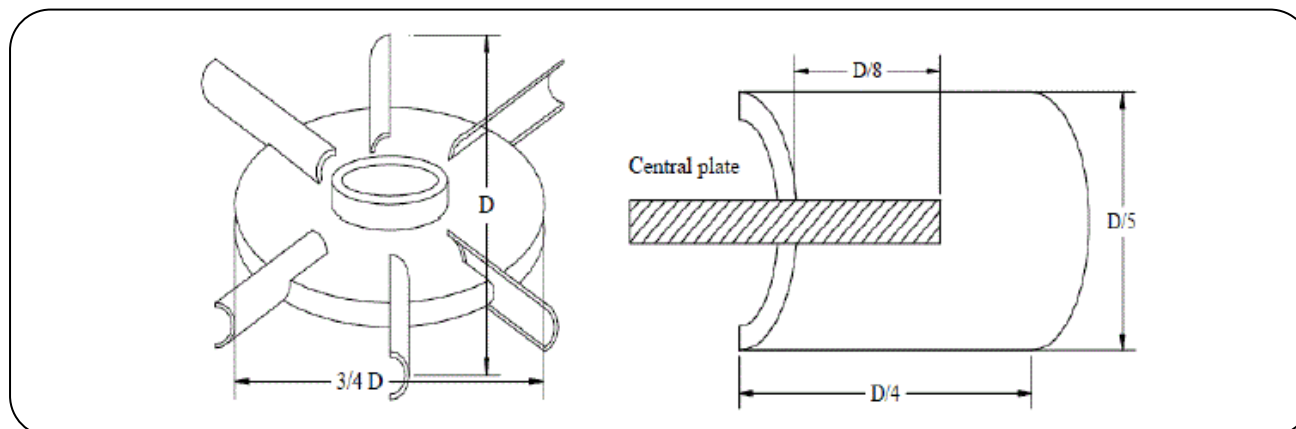
A physical method was chosen to measure the mass transfer coefficient in this work. As the solid particles are inert,

**Table 2: Details of the curved blade impeller.**

Specification	Length	Width	Swept area	Angle	Thickness
Values	D/4	D/5 (tip to tip distance)	$\pi D^2/40$	180°	3mm

**Table 3: List of symbols in the experimental apparatus.**

Symbol	Equipment	Symbol	Equipment
A	Pully	N	Manometer Tubes
B	Bearings	O	Manometer Tubes
C	Motor	P	Pressure Sensors
D	Impeller Coupler	Q	Digital Display
E	Shaft	R	Tachometer
F	Liquid level	S	Weight
G	Sparger	T	Level Arm
H	Tank	U	Load Cell
I	Rotameter	V	Recorder
J	Needle Valve	W	Invertor
K	Mirror Stand	X	Cable
L	Light	Y	Shaft
M	Manometer Scale		

**Fig. 1: Curved blade impeller.**

the mass transfer is only between the gaseous and liquid phases. The absorption of oxygen for the gaseous phase (air) to the liquid phase (water) was measured using a dissolved oxygen probe. The probe was accurate to 0.3 mg/L, while the resolution and range were 0.01 mg/L and 0-20 mg/L, respectively. The response time was less than 2 seconds. The probe was kept at a fixed location about 10 cm from the impeller near the tank wall. After

obtaining the DO values, the mass transfer was calculated using the following equation:

$$K_L a (C^* - C_t) = \frac{dC_t}{dt} \quad (1)$$

Where  $V$  is the liquid volume in the reactor,  $C^*$  is the saturated dissolved oxygen concentration and  $C_t$  is the dissolved oxygen concentration at any time  $t$  in the reactor. After integration, Eq (1) transforms to below:

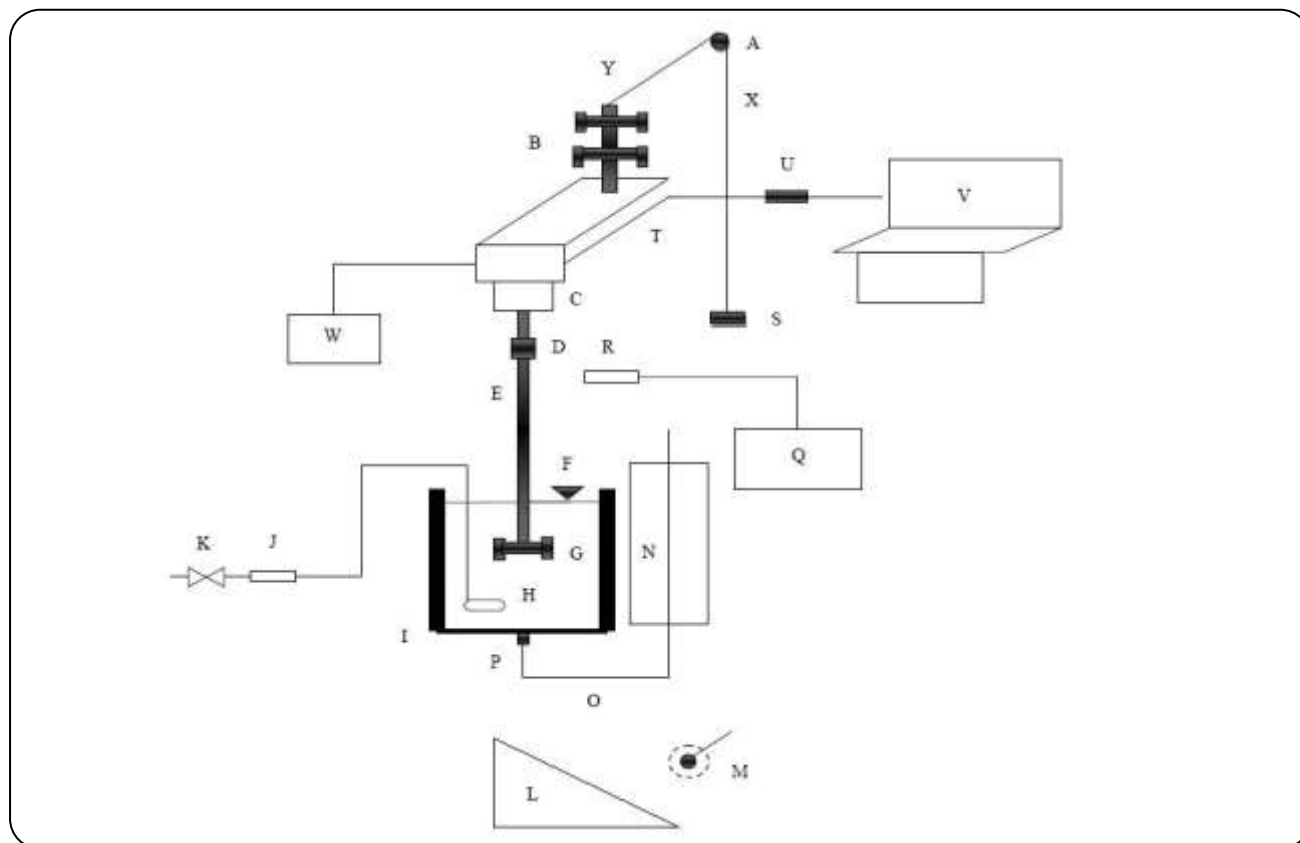


Fig. 2: Experimental setup.

$$\ln \left( \frac{C^* - C_0}{C^* - C_t} \right) = K_L a \cdot t \quad (2)$$

A plot of the left-hand side of Eq (2) against time provides a straight line with a slope of  $K_L a$ . The procedures of measuring the absorption of oxygen for the gaseous phase (air) to liquid phase (water) were used procedure was used for all experiments in this study.

### Modeling

Two artificial intelligence-based models, namely ANN and ANFIS, were designed in this study to map the four input parameters (number of curved blades, agitation speed, solid concentration, and superficial gas velocity) in relation to the mass transfer coefficient. ANFIS is a kind of neural network that integrates both ANN and fuzzy logic principles in a single framework.

#### Artificial Neural Networks

The history of ANN began with the pioneering work of McCulloch and Pitts [56] who had first introduced the idea of ANN as computing machines. ANN is a

computational system which follows the computational abilities of biological systems. Ability to find nonlinear and complex relationships has been the main reason for the ANN popularity in various areas such as image processing [57], document analysis [58], engineering tasks [59], financial modeling [60], and mass transfer studies [30-33].

A network consisting of multiple layers of artificial neurons is designed in order to determine the relationship between the experimental data. The first and last layers are called input and output layer, respectively. The in-between layers are known as hidden layers. Each of the neurons in the first layer receives information corresponding to one independent input variable. These neurons are simple and they process elements which transfer the receiving data to the output through the simple equation below:

$$O_i = f \left( \sum_{j=1}^n w_{ij} \cdot I_j + b_i \right) \quad (3)$$

where  $O_i$ ,  $f$ ,  $w_{ij}$ ,  $I_j$ ,  $b_i$ , and  $n$  refer to the output of the  $i$ th neuron, transfer function, a synaptic weight corresponding to the  $j$ th synapse of the  $i$ th neuron,  $j$ th input signal

Table 4: Geometrical dimensions of the used stirred vessel.

Descriptions	Size (Ratio)	Actual size (cm)
Tank diameter, T	T	40.0
Impeller clearance, C	T/3	13.3
Impeller diameter, D	T/3	13.3
Sparger diameter, S <sub>D</sub>	T/3	13.3
Sparger clearance, S	T/6	6.7
Liquid height, H	T	40.0
Baffle height, X	1.5T	60.0
Baffle width, B <sub>w</sub>	0.1T	4.0

to the  $i$ th neuron, the bias of the  $i$ th neuron, and the number of input signals to the  $i$ th neuron, respectively. The neurons inside the network are connected to each other by a direct communication link with associated weight ( $w_{ij}$ ).

The learning algorithm is another major factor that affects network performance. The neurons in each layer are connected to each other by communication links associated with connection weights. During ANN training, weights of the bonds are modified to decrease the calculated error. In general, different learning algorithms can be employed to establish the connection weights by minimizing the selected error function. In simple words, training a network is a process through which the values of weights and bias are adjusted. As stated before, in BNN technique weight and bias are updated in the direction of the negative gradient of the training error. The main types of BNNs are, Scaled Conjugate Gradient (SCG), Levenberg-Marquardt (LM), Gradient Descent with Momentum (GDA) and Resilient Back- Propagation (RP). In order to make sure the best possible network was selected, all variants were tested in this study during the training phase. The results obtained from different models were compared. The training parameters of the proposed ANN model are shown in Table 5.

#### Adaptive Neuro-Fuzzy Inference System (ANFIS)

ANFIS had been first proposed by Jang [35]. There are two types of inference systems in the fuzzy part, namely, zero or first-order Sugeno inference system and Tsukamoto inference system. By applying the defined fuzzy rules to input variables, output variables are achieved [35]:

Rule 1: if  $x$  is  $A_1$  and  $y$  is  $B_1$  the (4)

$$f_1 = p_1x + q_1y + r_1$$

Rule 2: if  $x$  is  $A_2$  and  $y$  is  $B_2$  the (5)

$$f_2 = p_2x + q_2y + r_2$$

where,  $p_1, p_2, q_1,$  and  $q_2$  are linear parameters while  $A_1, A_2, B_1,$  and  $B_2$  are nonlinear parameters.

The architecture of a two-input first-order Sugeno ANFIS model with two rules is depicted in Fig. 3. It is followed by the description of each layer and the function of their neurons.

The network includes 5 layers, namely, fuzzy layer, product layer, normalized layer, defuzzifier layer, and a total output layer. The four nodes of  $A_1, A_2, B_1,$  and  $B_2$  in the fuzzy layer represent linguistic labels in terms of fuzzy sets. They receive inputs  $x$  and  $y$ . By applying membership functions, the degree by which each input element belongs to the fuzzy sets is determined. The process can be shown as:

$$Q_{1,i} = \mu_{A_i}(X) \quad \text{for } i=1,2 \quad (6)$$

$$Q_{1,j} = \mu_{B_j}(Y) \quad \text{for } i=1,2 \quad (7)$$

Where  $X$  and  $Y$  are inputs to node 1 while  $A_i$  and  $B_j$  are the fuzzy sets.  $Q_{1,i}$  shows the membership degree of the input element.

The Gaussian curve and the generalized bell-shaped membership functions are among the most popular membership functions employed for  $\mu_{A_i}(X)$  and  $\mu_{B_j}(Y)$  [42].

**Table 5: Training parameters used for designing ANN.**

Property	Value
Learning algorithms	Levenberg-Marquardt Conjugate gradient Gradient descent with momentum Resilient Backpropagation
Minimized error function	Mean Square Error (MSE)
Learning	Supervised
Input layer transfer function	None
Hidden layer transfer function	Hyperbolic tangent sigmoid
Output layer transfer function	Linear
Number of training epochs (iterations)	200
Number of input neurons	3 (equal to number of input variables)
Number of hidden neurons	3-20
Number of output neurons	1 (equal to number of output variable)

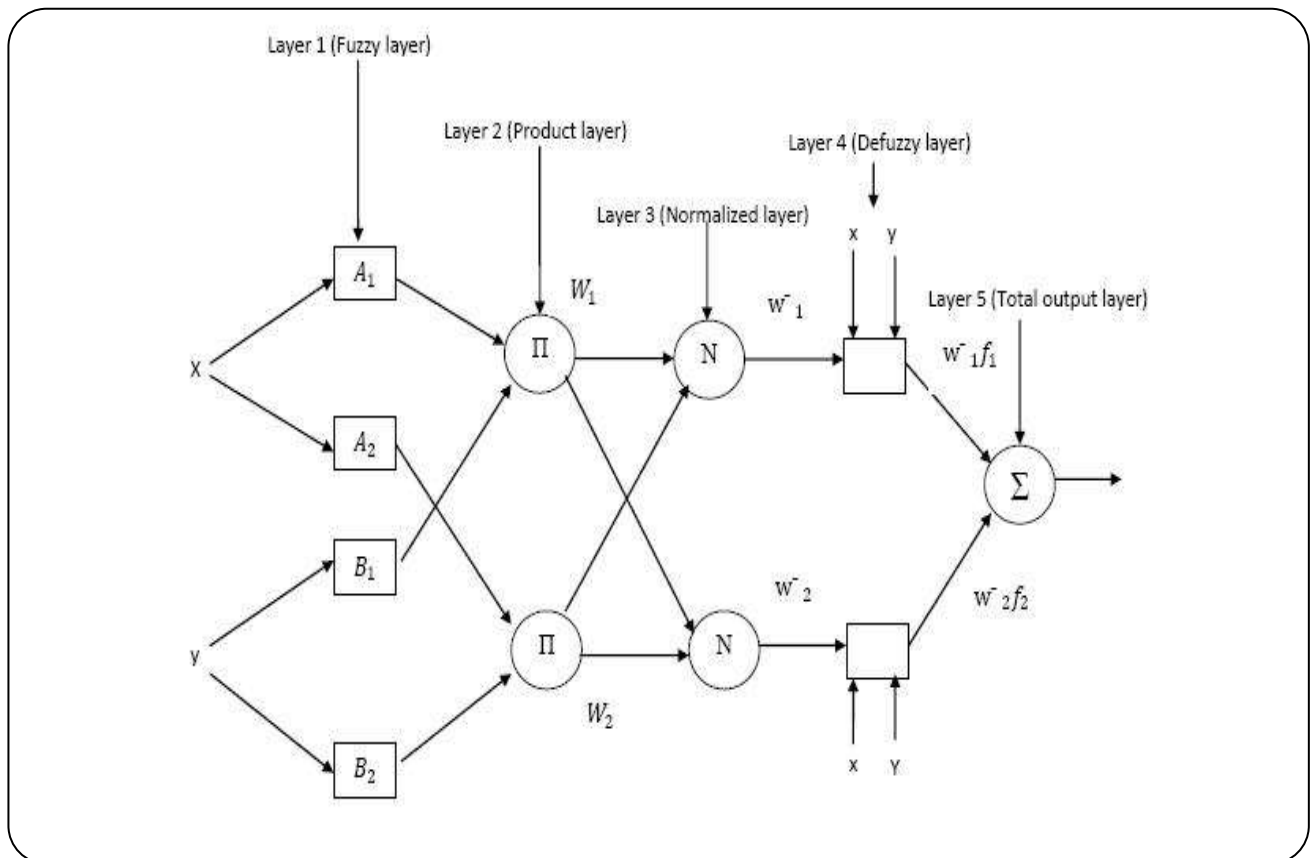


**Fig. 3: ANFIS architecture of a two input model with two rules.**

$$\mu_{A_i} = \frac{1}{1 + \left[ \left( \frac{x - c_i}{a_i} \right)^2 \right]^{b_i}} \quad (8)$$

$$\mu_{A_i}(X) = \exp \left[ - \left( \frac{x - c_i}{a_i} \right)^2 \right] \quad (9)$$

In these two equations,  $a_i$ ,  $b_i$ , and  $c_i$  refer to the set parameters.

The two nodes of the product layer with symbol 'Π' receive the generated signals of the previous layer and create the layer outputs ( $w_1$  and  $w_2$ ) through multiplying the signals. The produced outputs are weight functions of the normalized layer and can be shown as:

$$Q_{2,i} = w_i = \mu_{A_i}(x) \mu_{B_i}(y) \quad \text{for } i=1,2 \quad (10)$$

Where,  $Q_{2,i}$  represents the output of the product layer.

Nodes in the normalized layer are labeled with "N". The calculated  $Q_{2,i}$  in the previous layer demonstrates the firing strength of a rule. The  $i$ th node calculates the ratio of the  $i$ th rule's firing strength to the sum of all rules' firing strength. The normalized firing strength ( $Q_{3,i}$ ) is achieved by normalization of the weight function:

$$Q_{3,i} = \bar{w}_i = \frac{w_i}{w_1 + w_2} \quad \text{for } i=1,2 \quad (11)$$

The entering signals get fuzzified at the beginning of the process. During defuzzification, layer signals get defuzzified and they shift back to the normal form through the following formula:

$$Q_{4,i} = \bar{w}_i f_i = \bar{w}_i (p_i x + q_i y + r_i) \quad \text{for } i=1,2 \quad (12)$$

Where  $Q_{4,i}$ ,  $\bar{w}_i$ , and  $(p_i x + q_i y + r_i)$  stand for the output of layer four, the normalized firing strength from layer 3, and the set parameter, respectively.

The single node of the last layer with the symbol "Σ" computes the final decision as follows:

$$Q_{5,i} = \text{overall output} = \sum_i \bar{w}_i f_i = \frac{\sum_i w_i f_i}{\sum_i w_i} \quad (13)$$

ANFIS can use three different methodologies to generate the initial FIS. Genfis 1 produces initial FIS from the data using grid partitioning, while genfis 2 and

genfis 3 utilize subtractive clustering and fuzzy c-means clustering, respectively. Once the initial FIS is settled, the genfis accomplishes the modeling process by extracting some rules that describe the data behavior [35].

#### Statistical parameters

Five error functions were employed in order to determine the deviation of the model's results from the targets (experimental data). These statistical indicators are listed in Table 6.

#### Preprocessing

Pre-processing input data can improve network performance. During this process, input data are scaled to become more understandable for the network. For instance, reducing the dimension of input vectors can be fruitful when the components of the vectors are correlated (redundant). In this study, the principal component analysis [42] was utilized for processing the columns of the input matrix for both models.

## RESULTS AND DISCUSSION

### Experiment

Figs. 4 to 6 illustrate the obtained values in the experimental part of this study. In these figures, volumetric mass transfer coefficients are plotted versus the corresponding RPS for 4, 6, 8, and 12 curved blade impellers. The information is represented in three different superficial gas velocities.

### Parameter analysis

#### Effect of number of blades

Effect of the number of blades was studied in SC of 0.1 and  $U_g$  of 0.3 cm/s. The obtained  $k_L a$  for 4CB, 6CB, 8CB and 12 CB impellers in a wide range of agitation speeds are plotted in Fig. 6. 12CB produced the highest  $k_L a$  value at 12 RPS. 4CB produced slightly higher  $k_L a$  value compared to 8CB at 12 RPS. The lowest  $k_L a$  values were produced by 6CB and 4CB below 7 RPS while 12CB had the lowest  $k_L a$  value above the same agitation speed. Table 7 presents the achieved polynomial relationships for all four impellers.

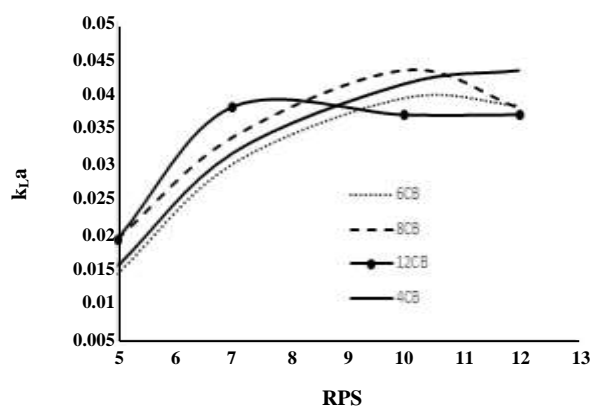
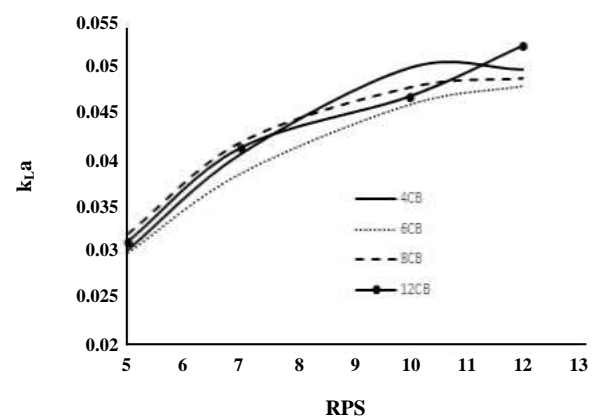
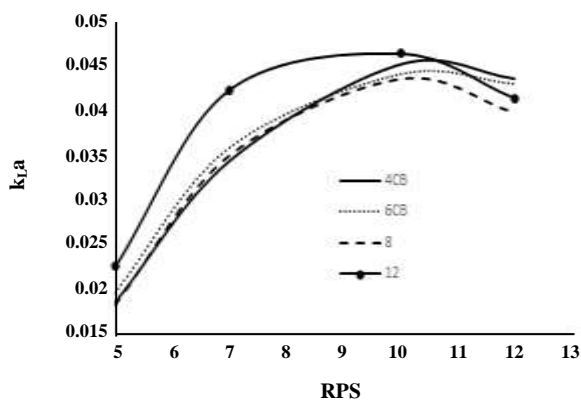
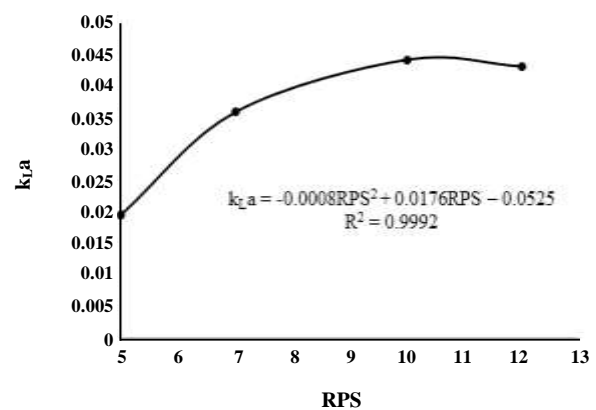
#### Effect of agitation speed

Fig. 7 shows the variation of  $k_L a$  values as a function of RPS at constant  $U_g$  of 0.2 cm/s and blade number of 6. These values increased in polynomial order with  $R^2$  equal to 0.9992.

Table 6: Error functions and their formula.

Error function	Equation	No.	Reference
Root mean square error	$RMSE = \sqrt{\frac{\sum_{i=1}^n (T_i - O_i)^2}{n}}$	14	[67]
Mean absolute error	$MAE = \frac{1}{n} \sum_{i=1}^n  T_i - O_i $	15	[29]
Absolute Average Deviation	$AAD\% = \frac{1}{n} \sum_{i=1}^n \left  \frac{T_i - O_i}{T_i} \right $	16	[68]
Pearson's cumulative test statistic	$\chi^2 = \sum_{i=1}^n \frac{(T_i - O_i)^2}{O_i}$	17	[69]
Correlation coefficient ( $R^2$ )	$R^2 = \frac{\sum_{i=1}^n (O_i - \bar{O})(T_i - \bar{T})}{\sum_{i=1}^n (O_i - \bar{O})^2}$	18	[70]

$n$ ,  $T$ ,  $O$ , and  $\bar{T}$  refer to the number of input patterns, experimental values (target), model's predictions (output), and average value of the experimental values, respectively

Fig. 4: Obtained  $k_{La}$  values in constant SC of 0.1 and  $U_g$  of 0.15 cm/s.Fig. 6: Obtained  $k_{La}$  values in constant SC of 0.1 and  $U_g$  of 0.3 cm/s.Fig. 5: Obtained  $k_{La}$  values in constant SC of 0.1 and  $U_g$  of 0.2 cm/s.Fig. 7:  $k_{La}$  values of 6CB impeller at various RPS and constant  $U_g$  of 0.2 cm/s.

As shown in Fig. 7,  $k_{La}$  value increased until certain agitation speed (10 RPS), beyond which the  $k_{La}$  value decreased.

#### Highest $k_{La}$ value

The maximum  $k_{La}$  values obtained in different conditions are listed in Table 8.

**Table 7: Polynomial relationships for all CB impellers.**

Impeller	Polynomial relationship	R <sup>2</sup>
4CB	$k_{La} = -0.0007RPS^2 + 0.015RPS - 0.0448$	0.9931
6CB	$k_{La} = -0.0007RPS^2 + 0.016RPS - 0.0463$	0.9967
8CB	$k_{La} = -0.0008RPS^2 + 0.017RPS - 0.046$	0.9993
12CB	$k_{La} = -0.0004RPS^2 + 0.010RPS - 0.0202$	0.9996

**Table 8: Maximum  $k_{La}$  values and their corresponding agitation speeds.**

Impeller	Condition					
	SC = 0.1					
	$U_g = 0.15$ cm/s		$U_g = 0.2$ cm/s		$U_g = 0.3$ cm/s	
	$k_{La}$	RPS	$k_{La}$	RPS	$k_{La}$	RPS
4CB	0.0433	12	0.0453	10	0.0501	10
6CB	0.0393	10	0.0442	10	0.0481	12
8CB	0.0434	10	0.0437	10	0.049	12
12CB	0.0381	7	0.0465	10	0.0525	12

**Table 9: Data statistics for the considered parameters for modeling.**

Modeling Subsets	Data statistics	Input parameters				Output parameter Volumetric mass transfer coefficient ( $k_{La}$ )
		Number of curved blades	Agitation speed (RPS)	Superficial gas velocity ( $U_g$ )	Solid concentration (%)	
Training set	Minimum	4	5	15	10	0.0143
	Maximum	12	12	30	20	0.0525
	Average	7.38	8.59	17.75	16.66	0.037
Testing Set	Minimum	4	5	15	10	0.0193
	Maximum	12	12	30	20	0.0501
	Average	8	8.11	20.62	16.66	0.0368
Overall Set	Minimum	4	5	15	10	0.0143
	Maximum	12	12	30	20	0.0525
	Average	7.5	8.5	18.23	16.66	0.037

As illustrated by Figs. 4-6 and indicated by Table 8, increasing agitation speed resulted in decreasing maximum  $k_{La}$  values when superficial gas velocity was equal to 0.15 cm/s. As  $U_g$  reached 0.2 cm/s, all four impellers showed their maximum  $k_{La}$  value at 10 RPS. Increasing  $U_g$  to 0.3 cm/s did not change the peak value for 4CB, but upgrade the maximum  $k_{La}$  value for the remaining three impellers at 12 RPS.

## Modeling

### Data set

Descriptive statistics of the considered parameters for both models are listed in Table 9.

### ANN

Both models were developed in the environment of MATLAB V7.0 (R14). The available data set was

divided into two groups: training and testing data set. During the model training, the network had access to both input and output variables to train itself. Meanwhile, in the testing phase, only the input data was received and the generated outputs were compared to the targets to evaluate the accuracy of the network's predictions.

The data portioning (training set, testing test, and cross-validation set) was carried out to reduce the risk of over-training and over-parameterization, and successful training was achieved when learning and cross-validation curves (MSE vs. epochs) approached to zero. Data division was done randomly to minimize errors due to possible systematic trends in variables.

As discussed before, there are various learning algorithms to train a neural network. The four most commonly used algorithms were chosen in this study to train the network. Besides, the number of neurons in hidden-layer varied from 3 to 20 in each learning algorithm. It was hoped that the diversity of learning algorithms and number of neurons in hidden layer could lead to the development of the best possible neural network as this was a common procedure in the previously published reports [28-30].

The performance of the resulting networks was compared to each other to select the best network in terms of mean square error criteria. The recorded results in epoch 50 are listed in Table 10.

As observed from Table 10, a three-layer neural network with 7 neurons in hidden layer that followed Levenberge Marquardt learning algorithm offered the least test error (5.04) compared to the other networks and was therefore chosen as the most reliable ANN model. As elaborated before, the neural networks have access to both input and target data during the training phase, while only input data are provided during the test phase. That would explain the notable difference in the MSE values between the training and testing phase for each network developed. Systematically, the MSE values of the networks designed with RB algorithm started increasing with an increase in the number of hidden neurons up to a certain number (10); and henceforth, MSE values tend to decrease. The networks developed by other algorithms did not exhibit the same discipline. The most accurate networks created by RB, SCG, and GDA algorithms achieved the MSE values of 9.26, 5.34, and 5.3 with corresponding hidden neuron numbers of 3, 6, and 4

respectively. Fig. 8 represents the structure of the proposed ANN model of this study. Later, this model was compared with the proposed neuro-fuzzy model in terms of prediction accuracy.

#### ANFIS

Subtractive clustering has been employed for developing initial FIS models as the superior speed and ability of this partitioning technique in capturing the complex relationship between the input and output variables has been determined in previous studies [42]. Once the parameters of subtractive clustering, namely, the range of influence (ROI), Squash Factor (SF), Accept Ratio (AR), and reject ratio (RR) are optimized, the most reliable model can be obtained. In this study, the initial FIS was designed by the initial values of the clustering parameters (ROI=0.5, SF=1.25, AR=0.5, and RR=0.15). Thereafter, the created ANFIS's model was modified by changing the values of the clustering parameters around their default numbers until the best performance (in terms of RMSE) was achieved. Then, the remaining three parameters were held constant in their default values, resulting in four computational groups in order to optimize each parameter. In the first test, for instance, the effect of ROI was examined in a range of 0.4-0.6 while values of SF, AR, and RR were kept at default values of 1.25, 0.5, and 0.15, respectively. The investigation ranges of SF, AR, and RR were fixed as 1.2-1.36, 0.45-0.55, and 0.1-0.2 respectively. Once the optimal value for a particular parameter was discovered, it was used as the value of the corresponding parameter in the next test, replacing the default value. Fig. 9 reflects the variations in RMSE for different values of clustering parameters for testing data. Data are recorded in the epoch number of 10.

Evidently, all clustering parameters except AR had a significant impact on the accuracy of the neuro-fuzzy network. Therefore, there is no need to update the initial values of AR. Conversely, Figs. 9(a), 9(b), and 9(d) demonstrate that increasing the values of ROI, SF, and RR had a considerable impact on RMSE values. As a result, the values of ROI, SF, and RR were changed to 0.46, 1.32, and 0.18 respectively in order to have the most accurate model. Finally, the optimum neuro-fuzzy structure (ROI=0.46, SF=1.32, AR=0.5, and RR=0.18) for forecasting  $k_L a$  value in a curved blade Rushton turbine stirred vessel is depicted in Fig. 10. The RMSE values

Table 10: Performances of various designed neural networks.

Algorithm	Neurons number in hidden layer	MSE	
		Training	Test
Resilient Backpropagation	3	1.07	9.26
Resilient Backpropagation	4	2.19	10.73
Resilient Backpropagation	5	2.97	13.35
Resilient Backpropagation	6	4.79	15.21
Resilient Backpropagation	7	3.06	15.45
Resilient Backpropagation	8	3.29	18.79
Resilient Backpropagation	9	4.11	19.26
Resilient Backpropagation	10	4.43	22.99
Resilient Backpropagation	15	1.53	13.01
Resilient Backpropagation	20	1.09	12.84
LevenbergeMarquardt	3	1.35	10.8
LevenbergeMarquardt	4	0.99	6.2
LevenbergeMarquardt	5	2.91	7.9
LevenbergeMarquardt	6	0.02	5.21
LevenbergeMarquardt	7	0.13	5.04
LevenbergeMarquardt	8	6.76	13.07
LevenbergeMarquardt	9	7.03	12.78
LevenbergeMarquardt	10	8.93	19.24
LevenbergeMarquardt	15	7.90	21.79
LevenbergeMarquardt	20	6.09	17.89
Scaled conjugate gradient	3	4.86	10.54
Scaled conjugate gradient	4	1.11	9.03
Scaled conjugate gradient	5	1.04	10.98
Scaled conjugate gradient	6	0.09	5.34
Scaled conjugate gradient	7	1.02	8.98
Scaled conjugate gradient	8	1.09	8.88
Scaled conjugate gradient	9	1.10	8.40
Scaled conjugate gradient	10	1.12	8.98
Scaled conjugate gradient	15	1.15	7.57
Scaled conjugate gradient	20	3.18	17.09
Gradient descent with momentum	3	2.54	10.86
Gradient descent with momentum	4	0.16	5.3
Gradient descent with momentum	5	1.71	7.57
Gradient descent with momentum	6	1.29	5.35
Gradient descent with momentum	7	2.23	6.99
Gradient descent with momentum	8	2.01	6.14
Gradient descent with momentum	9	1.57	20.34
Gradient descent with momentum	10	0.98	11.21
Gradient descent with momentum	15	0.13	20.75
Gradient descent with momentum	20	0.19	8.54

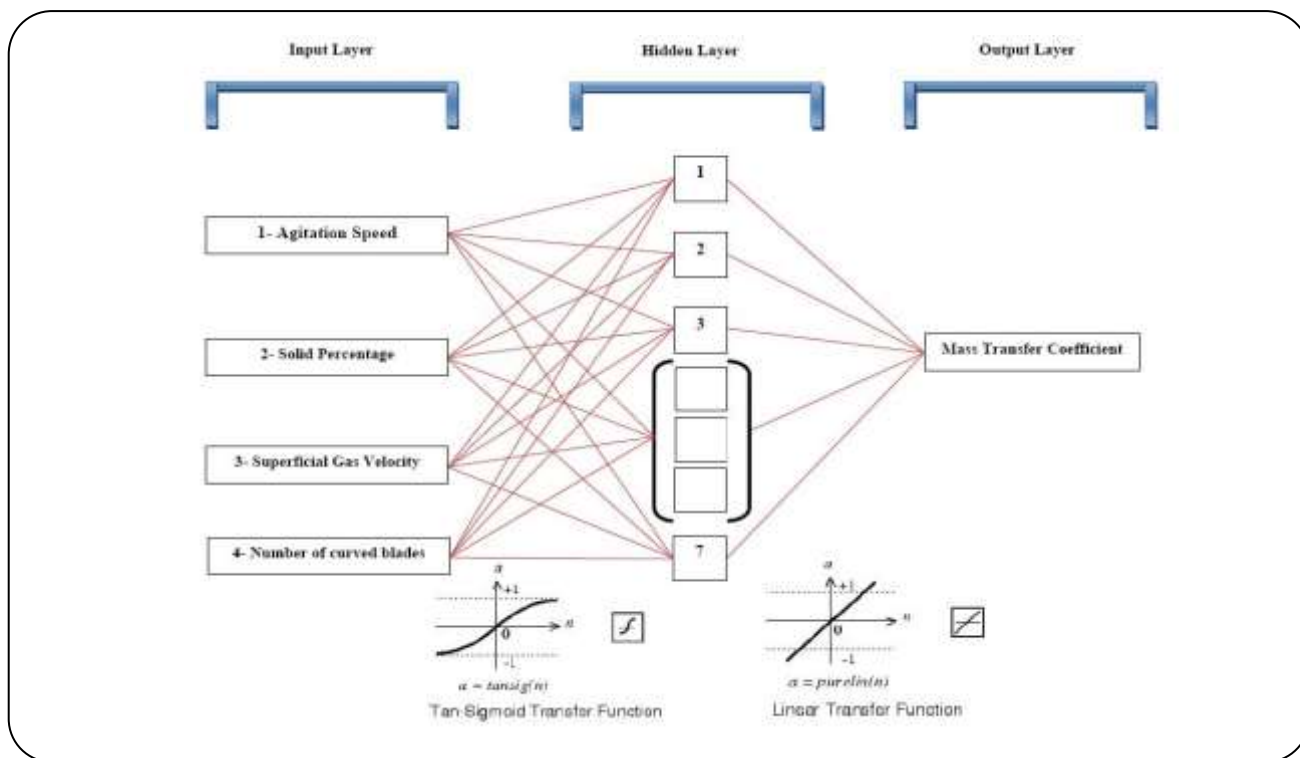


Fig. 8: Structure of the most accurate neural network.

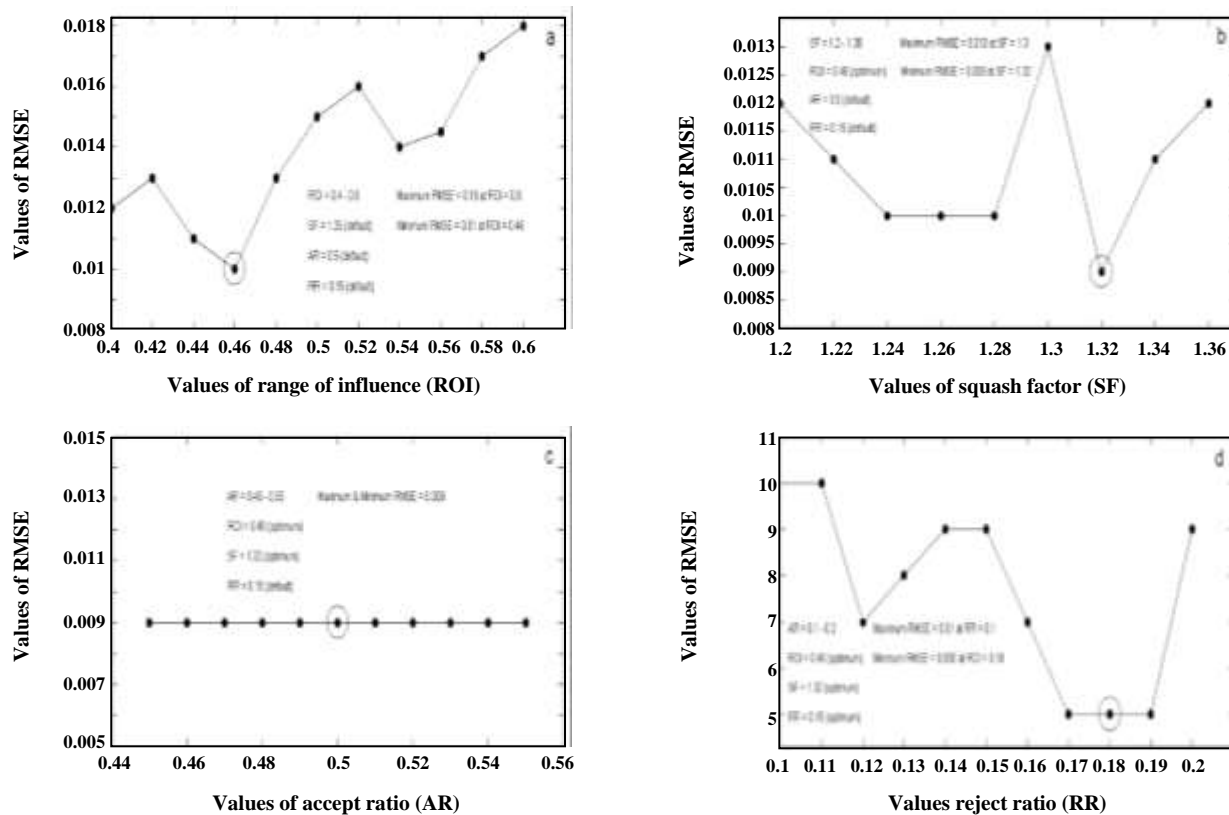


Fig. 9: Effect of clustering parameters (ROI (a), SF (b), AR(c), and RR (d)) on model's performance.

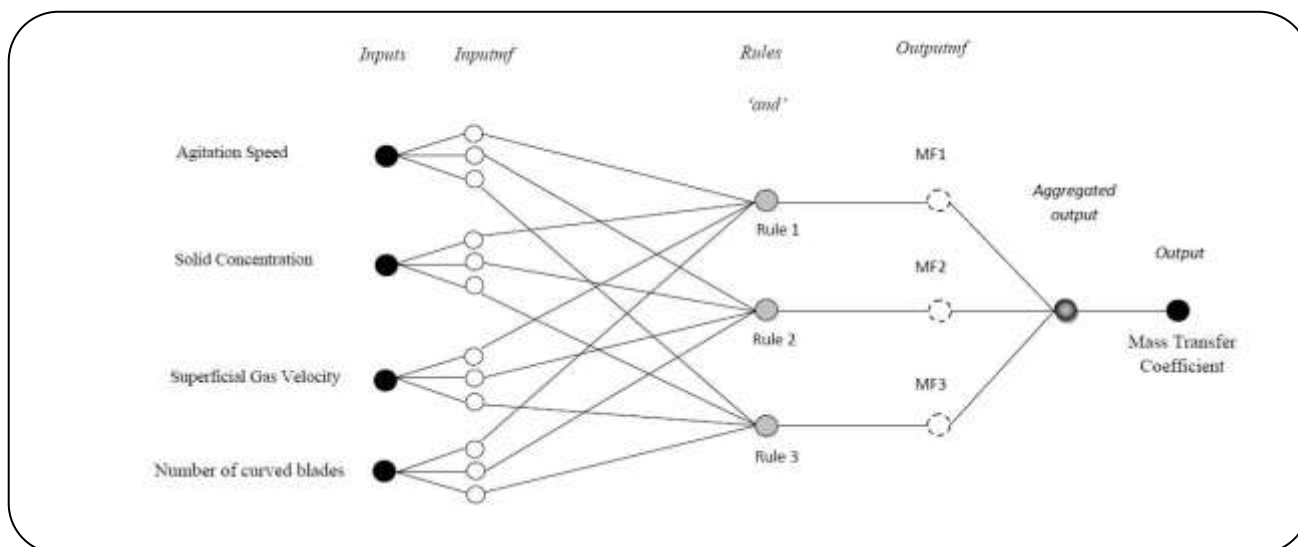


Fig. 10: Structure of the optimum ANFIS mod.

before and after the modification process were 0.015 and 0.009 respectively. The final value of RMSE indicates excellent agreement between ANFIS outputs and their targets (experimental data).

#### Comparing the proposed models

Performances of the two proposed models in this study (ANN and ANFIS) were examined by comparing the correctness of the predicted results. Five different performance indicators listed in Table 6 were employed in order to assure the judgment. Table 11 represents the findings.

In Table 11 and Fig. 11, the prediction results of both models were compared for the training, testing, and overall data. Since only 10% of the available data was put to test, the error values for the overall data were closer to those of the training data. However, it should be noted that the recorded error values in the testing phase have the main role in identifying the accuracy of any designed model. As observed in Table 11, all indices clearly indicated that the proposed ANFIS's model generated more accurate outputs with less deviation from the targets. ANFIS's model exhibited superior predictive ability in forecasting the volumetric mass transfer coefficient in this study compared to the created ANN's model. In the testing part, the correlation coefficient suggests that 99.01% of the total variations were explained by the neuro-fuzzy model, while 3.88% of the total predictions did not follow the experimental data in

ANN. Comparison of the reported error values with the other indices reported the same dominant performance of ANFIS-based models.

Further comparison is made in Fig 11, in which deviations between the predictions done by ANFIS's and ANN's model are plotted for all experimental samples.

As exhibited by Fig. 11, predictions of the ANN-based model were not as precise as those of ANFIS's model. The recorded values in Table 11 and the graphical comparison presented in Fig. 11 clearly ascertain that the ANFIS-based model implied more satisfactory predictions and hence was selected as the reliable model. Moreover, the developed ANFIS's model in this study presented more satisfactory predictions compared to the ANN's and RSM's models as listed in Table 1.

#### CONCLUSIONS

In this study, experiments were carried out to identify the volumetric mass transfer coefficient in three-phase systems. Experimental data was gathered to design two artificial intelligence-based models, using artificial neural networks and adaptive neuro-fuzzy inference system, respectively, for mapping four input variables to  $k_{L,a}$ . The comparison showed that ANFIS's model had better performance. The achievements of this study can be summarised as follows:

- Mass transfer coefficient,  $k_{L,a}$ , in a curved blade agitated stirred vessel was determined in various operational and geometrical conditions (agitation speeds

Table 11: Comparing accuracy of the developed models.

Performance indices	Train		Test		Overall	
	ANN	ANFIS	ANN	ANFIS	ANN	ANFIS
MAE	0.088	0.0032	0.104	0.0051	0.093	0.0035
RMSE	0.765	0.0043	0.867	0.0059	0.0802	0.0046
AAD%	7.83	1.22	8.04	1.82	7.87	1.33
$\chi^2$	0.074	0.0014	0.096	0.0019	0.081	0.0015
R <sup>2</sup>	0.9603	0.9947	0.9512	0.9901	0.9578	0.9941

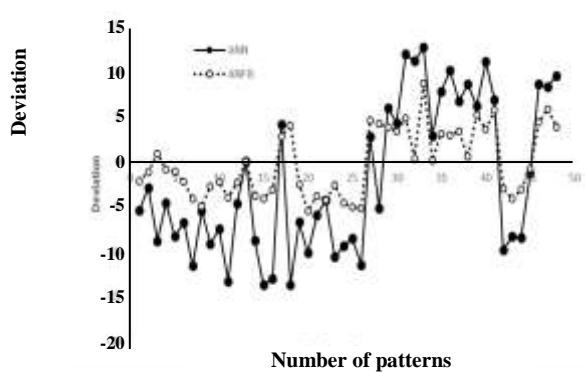


Fig. 11: Deviations of the proposed models.

of 5, 7, 10, 12 RPS, superficial gas velocities of 0.15, 0.2, 0.3 cm/s, solid concentrations of 0.1, 0.2, and curved blade numbers of 4, 6, 8, and 12).

- ANFIS was employed to develop a reliable model to map four input variables to  $k_{L,a}$  using the selected experimental data. The proposed model was able to predict the data not utilized for training with a correlation coefficient of 0.9901.

- Based on the same data set, another model was developed by ANN. The performance indices such as MAE, RMSE, AAD%,  $\chi^2$ , and R<sup>2</sup> demonstrated superior efficiency of the ANFIS's model over ANN's model. In the testing part where the accuracy of the models' predictions was examined, AAD% of 1.82 revealed that most of the total variations were explained by the ANFIS's model, while AAD% was equal to 8.04 for the ANN's model

- Modeling of multi-phase systems in stirred vessels are complex and challenging as several different phenomena are taking place simultaneously. This study determined the efficiency of ANFIS in approximating the system behavior and predicting  $k_{L,a}$  values. The authors are optimistic

that ANFIS can be used in similar modeling and optimization studies based on satisfactory results in this study.

- More effective parameters can be used for training ANFIS network. If another geometrical parameter such as vessel volume can be included in the training data set, the built ANFIS's model could be scaled up.

#### Acknowledgment

This research is supported by a Postgraduate Research Fund (PPP) with project number PG115- 2012B from the University of Malaya.

Received: Jun. 13, 2017 ; Accepted: Oct. 16, 2017

#### REFERENCES

- [1] Nienow A., Konno M., Bujalski W., [Studies on Three-Phase Mixing: A Review and Recent Results](#), *Chemical Engineering Research & Design*, **64**(1): 35-42 (1986).
- [2] Frijlink J., Bakker A., Smith J., [Suspension of Solid Particles with Gassed Impellers](#), *Chemical Engineering Science*, **45**(7): 1703-1718 (1990).
- [3] Rewatkar V.B., Rao K.R., Joshi J.B., Critical Impeller Speed for Solid Suspension in Mechanically Agitated Three-Phase Reactors. 1. Experimental Part, *Industrial & Engineering Chemistry Research*, **30**(8): 1770-1784 (1991).
- [4] Dutta N., Pangarkar V., [Critical Impeller Speed for Solid Suspension in Multi-Impeller Three Phase Agitated Contactors](#), *The Canadian Journal of Chemical Engineering*, **73**(3): 273-283 (1995).
- [5] Saravanan K., Patwardhan A., Joshi J., [Critical Impeller Speed for Solid Suspension in Gas Inducing Type Mechanically Agitated Contactors](#), *The Canadian Journal of Chemical Engineering*, **75**(4): 664-676 (1997).

- [6] Doran P.M., [Design of Mixing Systems for Plant Cell Suspensions in Stirred Reactors](#), *Biotechnology Progress*, **15**(3): 319-335 (1999).
- [7] Dohi N., Matsuda Y., Itano N., Minekawa K., Takahashi T., Kawase Y., [Suspension of Solid Particles in Multi-Impeller Three-Phase Stirred Tank Reactors](#), *The Canadian Journal of Chemical Engineering*, **79**(1): 107-111 (2001).
- [8] Fishwick R., Winterbottom J., Stitt E., [Effect of Gassing Rate on Solid-Liquid Mass Transfer Coefficients and Particle Slip Velocities in Stirred Tank Reactors](#), *Chemical Engineering Science*, **58**(3): 1087-1093 (2003).
- [9] Kluytmans J.H., van Wachem B.G.M., Kuster M., Schouten J.C., [Mass Transfer in Sparged and Stirred Reactors: Influence of Carbon Particles and Electrolyte](#), *Chemical Engineering Science*, **58**(20): 4719-4728 (2003).
- [10] Martín M., Montes F.J., Galán M.A., [Mass Transfer Rates From Bubbles in Stirred Tanks Operating with Viscous Fluids](#), *Chemical Engineering Science*, **65**(12): 3814-3824 (2010).
- [11] Danckwerts P.V., Lannus A., [Gas-Liquid Reactions](#), *Journal of the Electrochemical Society*, **117**(10): 369C-370C (1970).
- [12] Van't Riet K., [Review of Measuring Methods and Results in Nonviscous Gas-Liquid Mass Transfer in Stirred Vessels](#), *Industrial & Engineering Chemistry Process Design and Development*, **18**(3): 357-364 (1979).
- [13] Beenackers A., Van Swaaij W., [Mass Transfer in Gas-Liquid Slurry Reactors](#), *Chemical Engineering Science*, **48**(18): 3109-3139 (1993).
- [14] Nienow A.W., "Aeration, Biotechnology", In: Kirk-Othmer Encyclopedia of Chemical Technology, (2003).
- [15] Puthli M.S., Rathod V.K., Pandit A.B., [Gas-Liquid Mass Transfer Studies with Triple Impeller System on a Laboratory Scale Bioreactor](#), *Biochemical Engineering Journal*, **23**(1): 25-30 (2005).
- [16] Garcia-Ochoa F., Gomez E., [Bioreactor Scale-up and Oxygen Transfer Rate in Microbial Processes: an Overview](#), *Biotechnology Advances*, **27**(2): 153-176 (2009).
- [17] Nigam K.D., Schumpe A., "Three-Phase Sparged Reactors", (1996).
- [18] Conway K., Kyle A., Rielly C.D., [Gas-Liquid-Solid Operation of a Vortex-Ingesting Stirred Tank Reactor](#), *Chemical Engineering Research and Design*, **80**(8): 839-845 (2002).
- [19] Mehta V., Sharma M., [Mass Transfer in Mechanically Agitated Gas-Liquid Contactors](#), *Chemical Engineering Science*, **26**(3): 461-479 (1971).
- [20] Gentile F., Oleschko H., Veverka P., Machoň V., Paglianti A., Bujalski W., Etchells A.W., Nienow A.W., [Some Effects of Particle Wettability in Agitated Solid-Gas-Liquid Systems: Gas-Liquid Mass Transfer and the Dispersion of Floating Solids](#), *The Canadian Journal of Chemical Engineering*, **81**(3-4): 581-587 (2003).
- [21] Rawase Y., Araki T., Shimzu K., Miura H., [Gas-Liquid Mass Transfer in Three-Phase Stirred Tank Reactors: Newtonian and Non-Newtonian Fluids](#), *The Canadian Journal of Chemical Engineering*, **75**(6): 1159-1164 (1997).
- [22] Tagawa A., Dohi N., Kawase Y., [Volumetric Gas-Liquid Mass Transfer Coefficient in Aerated Stirred Tank Reactors with Dense Floating Solid Particles](#), *Industrial & Engineering Chemistry Research*, **51**(4): 1938-1948 (2011).
- [23] Robinson C.W., Wilke C.R., [Oxygen Absorption in Stirred Tanks: A Correlation for Ionic Strength Effects](#), *Biotechnology and Bioengineering*, **15**(4): 755-782 (1973).
- [24] Robinson C.W., Wilke C.R., [Simultaneous Measurement of Interfacial Area and Mass Transfer Coefficients for a Well-Mixed Gas Dispersion in Aqueous Electrolyte Solutions](#), *AIChE Journal*, **20**(2): 285-294 (1974).
- [25] Hassan I.T.M., Robinson C.W., [Oxygen Transfer in Mechanically Agitated Aqueous Systems Containing Dispersed Hydrocarbon](#), *Biotechnology and Bioengineering*, **19**(5): 661-682 (1977).
- [26] Hassan I.T.M., Robinson C.W., [Measurement of Bubble Size Distribution in Turbulent Gas-Liquid Dispersions](#), *Chemical Engineering Research & Design*, : 62- (1984).
- [27] Kralj F., Sinčić D., [Hold-up and Mass Transfer in a Two- and Three-Phase Stirred Tank Reactor](#), *Chemical Engineering Science*, **39**(3): 604-607 (1984).

- [28] Iglesias Nuno A., Arcay B., Cotos J.M., Varela J., Optimisation of Fishing Predictions by Means of Artificial Neural Networks, *Anfis, Functional Networks and Remote Sensing Images, Expert Systems with Applications*, **29**(2): 356-363 (2005).
- [29] Prakash Maran J., Sivakumar V., Thirugnanasambandham K., Sridhar R., Artificial Neural Network and Response Surface Methodology Modeling in Mass Transfer Parameters Predictions During Osmotic Dehydration of Carica Papaya L., *Alexandria Engineering Journal*, **52**(3): 507-516 (2013).
- [30] Lertworasirikul S., Saetan S., Artificial Neural Network Modeling of Mass Transfer During Osmotic Dehydration of Kaffir Lime Peel, *Journal of Food Engineering*, **98**(2): 214-223 (2010).
- [31] García-Ochoa F., Castro E.G., Estimation of Oxygen Mass Transfer Coefficient in Stirred Tank Reactors Using Artificial Neural Networks, *Enzyme and Microbial Technology*, **28**(6): 560-569 (2001).
- [32] Fu K., Chen G., Sema T., Zhang X., Liang Z., Idem R., Tontiwachwuthikul P., Experimental Study on Mass Transfer and Prediction Using Artificial Neural Network for CO<sub>2</sub> Absorption into Aqueous DETA, *Chemical Engineering Science*, **100**(0): 195-202 (2013).
- [33] Ochoa-Martínez C.I., Ayala-Aponte A.A., Prediction of Mass Transfer Kinetics During Osmotic Dehydration of Apples Using Neural Networks, *LWT - Food Science and Technology*, **40**(4): 638-645 (2007).
- [34] Wieland D., Wotawa F., Wotawa G., From Neural Networks to Qualitative Models in Environmental Engineering, *Computer-Aided Civil and Infrastructure Engineering*, **17**(2): 104-118 (2002).
- [35] Jang J.S.R., ANFIS: Adaptive-Network-Based Fuzzy Inference System, *IEEE Transactions on Systems, Man, and Cybernetics*, **23**: 665-685 (1993).
- [36] Rahmanian B., Pakizeh M., Mansoori S.A.A., Estandyari M., Jafari D., Maddah H., Maskooki A., Prediction of MEUF Process Performance Using Artificial Neural Networks and ANFIS Approaches, *Journal of the Taiwan Institute of Chemical Engineers*, **43**(4): 558-565 (2012).
- [37] Mehrabi M., Pesteei S.M., Pashae G T., Modeling of Heat Transfer and Fluid Flow Characteristics of Helicoidal Double-Pipe Heat Exchangers Using Adaptive Neuro-Fuzzy Inference System (ANFIS), *International Communications in Heat and Mass Transfer*, **38**(4): 525-532 (2011).
- [38] Rezaei E., Karami A., Yousefi T., Mahmoudnezhad S., Modeling the Free Convection Heat Transfer in a Partitioned Cavity Using ANFIS, *International Communications in Heat and Mass Transfer*, **39**(3): 470-475 (2012).
- [39] Mullai P., Arulselvi SA., Ngo H.H., Sabarathinam P.L., Experiments and ANFIS Modelling for the Biodegradation of Penicillin-G Wastewater Using Anaerobic Hybrid Reactor, *Bioresource Technology*, **102**(9): 5492-5497 (2011).
- [40] Khazraee S.M., Jahanmiri A.H., Composition Estimation of Reactive Batch Distillation by Using Adaptive Neuro-Fuzzy Inference System, *Chinese Journal of Chemical Engineering*, **18**(4): 703-710 (2010).
- [41] Heidari E., Ghoreishi S.M., Prediction of Supercritical Extraction Recovery of EGCG Using Hybrid of Adaptive Neuro-Fuzzy Inference System and Mathematical Model, *The Journal of Supercritical Fluids*, **82**(0): 158-167 (2013).
- [42] Yetilmezsoy K., Fingas M., Fieldhouse B., An Adaptive Neuro-Fuzzy Approach for Modeling of Water-in-Oil Emulsion Formation, *Colloids and Surfaces A: Physicochemical and Engineering Aspects*, **389**(1-3): 50-62 (2011).
- [43] Moon J.W., Jung S.K., Kim Y., Han S.H., Comparative Study of Artificial Intelligence-Based Building Thermal Control Methods – Application of Fuzzy, Adaptive Neuro-Fuzzy Inference System, and Artificial Neural Network, *Applied Thermal Engineering*, **31**(14-15): 2422-2429 (2011).
- [44] Varol Y., Avci E., Koca A., Oztop H.F., Prediction of Flow Fields and Temperature Distributions Due to Natural Convection in a Triangular Enclosure Using Adaptive-Network-Based Fuzzy Inference System (ANFIS) and Artificial Neural Network (ANN), *International Communications in Heat and Mass Transfer*, **34**(7): 887-896 (2007).

- [45] Rahman M.S., Rashid M.M., Hussain M.A., [Thermal Conductivity Prediction of Foods by Neural Network and Fuzzy \(ANFIS\) Modeling Techniques](#), *Food and Bioproducts Processing*, **90**(2): 333-340 (2012).
- [46] Van Weert G., Van Der Werff D., Derksen J.J., [Transfer of O<sub>2</sub> From Air to Mineral Slurries in a Rushton Turbine Agitated Tank](#), *Minerals Engineering*, **8**(10): 1109-1124 (1995).
- [47] Guillard F., Trägårdh C., [Mixing in Industrial Rushton Turbine-Agitated Reactors under Aerated Conditions](#), *Chemical Engineering and Processing: Process Intensification*, **42**(5): 373-386 (2003).
- [48] Yapici K., Karasozen B., Schäfer M., Uludag S., [Numerical investigation of the Effect of the Rushton Type Turbine Design Factors on Agitated Tank Flow Characteristics](#), *Chemical Engineering and Processing: Process Intensification*, **47**(8): 1340-1349 (2008).
- [49] Taghavi M., [Experimental and CFD Investigation of Power Consumption in a Dual Rushton Turbine Stirred Tank](#), *Chemical Engineering Research and Design*, **89**(3): 280-290 (2011).
- [50] Wu H., Arcella V., Malavasi M., [A Study of Gas-Liquid Mass Transfer in Reactors with Two Disk Turbines](#), *Chemical Engineering Science*, **53**(5): 1089-1095 (1998).
- [51] Ochieng A., Onyango M.S., Kumar A., Kiriamiti K., Musonge P., [Mixing in a Tank Stirred by a Rushton Turbine at a Low Clearance](#), *Chemical Engineering and Processing: Process Intensification*, **47**(5): 842-851 (2008).
- [52] Nienow A.W., [Gas-Liquid Mixing Studies: A Comparison of Rushton Turbine with Some Modern Impellers](#), *Trans, IChemE*, **74**: 417-423 (1996).
- [53] Van't Riet K., Smith J.M., [The Behaviors of Gas-Liquid Mixtures Near Rushton Turbine Blades](#), *Chemical Engineering Science*, **28**: 1031-1037 (1993).
- [54] Van't Riet K., Boom J.M., Smith J.M., [Power Consumption, Impeller Coalescence and Recirculation in Aerated Vessels](#), *Chemical Engineering Research and Design*, **54**: 124-131 (1976).
- [55] Warmoeskerken M.M.C.G., Smith J.M., [The Hallow Blade Agitator for Dispersion and Mass Transfer](#), *Chemical Engineering Science*, **67**: 193-198 (1989).
- [56] McCulloch W.S., Pitts W., [A Logical Calculus of the Ideas Immanent in Nervous Activity](#), *Bulletin of Mathematical Biophysics*, **9**: 127-147 (1943).
- [57] Duranton M., [Image Processing by Neural Networks](#), *Micro IEEE*, **12-19** (1996).
- [58] Marinai S., [Artificial Neural Networks for document Analysis and Recognition](#), *IEEE Transactions on Pattern Analysis and Machine Intelligence*, **7**: 23-35 (2005).
- [59] Zhenyuan W., Yilu L., [Neural Network and Expert System Diagnose Transformer Faults](#), *IEEE Computer Applications in Power*, **12**: 50-55 (2000).
- [60] Abu-Mostafa Y.S., [Financial Model Calibration Using Consistency Hints](#), *IEEE Transactions on Neural Networks*, **12**: 791-808 (2001).